

LATENT ASSISTANCE NETWORKS: REDISCOVERING HYPERBOLIC TANGENTS IN RL

Jacob E. Kooi, Mark Hoogendoorn & Vincent François-lavet

Department of Computer Science
Vrije Universiteit Amsterdam
Amsterdam, Netherlands.
j.e.kooi@vu.nl

ABSTRACT

Activation functions are one of the key components of a neural network. The most commonly used activation functions can be classed into the category of continuously differentiable (e.g. tanh) and linear-unit functions (e.g. ReLU), both having their own strengths and drawbacks with respect to downstream performance and representation capacity through learning (e.g. measured by the number of dead neurons and the effective rank). In reinforcement learning, the performance of continuously differentiable activations often falls short as compared to linear-unit functions. From the perspective of the activations in the last hidden layer, this paper provides insights regarding this sub-optimality and explores how activation functions influence the occurrence of dead neurons and the magnitude of the effective rank. Additionally, a novel neural architecture is proposed that leverages the product of independent activation values. In the Atari domain, we show faster learning, a reduction in dead neurons and increased effective rank.

1 INTRODUCTION

Out of all activation functions, the Rectified Linear Unit (ReLU) (Nair & Hinton, 2010) and its variants (Xu et al., 2015; Klambauer et al., 2017) have emerged as the most widely used and generally best-performing activation functions up until this day (Jarrett et al., 2009; Goodfellow et al., 2016). The strength of the ReLU activation lies in its ability to naturally avoid vanishing gradients when used in deeper networks, in contrast to the continuously differentiable activation functions, such as the sigmoid and the hyperbolic tangent (Glorot & Bengio, 2010).

A common drawback of using the ReLU activation is its limited expressivity in the context of shallow networks (see Figure 2), as well as the phenomenon known as the dying ReLU problem (He et al., 2015; Lu et al., 2019). As training progresses, the number of dying ReLU’s tend to increase, resulting in a dying network (Dubey et al., 2022).

In reinforcement learning (RL) (Sutton & Barto, 2018), even though training results in a large number of dying ReLU’s (Gulcehre et al., 2022; Sokar et al., 2023), the ReLU function remains the most popular activation for performance reasons (Henderson et al., 2018). As a result, continuously differentiable activation functions like the hyperbolic tangent are rarely used (see Fig. 1), even though their symmetrical, bounded shape and smooth gradient landscape has advantages for optimization. Not much attention has been given to investigate and provide a solution to this mysterious lack of performance, despite evidence showing that a hidden layer activated by a hyperbolic tangent is

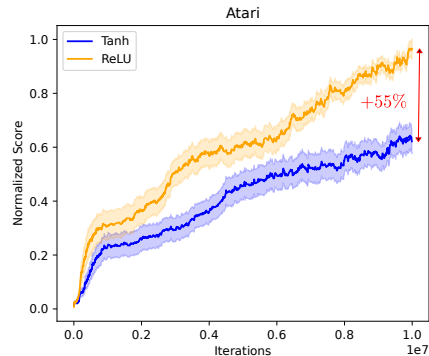


Figure 1: Normalized performance training DQN in the Atari domain where the activation of the representation, defined as the final hidden layer, is either ReLU or tanh.

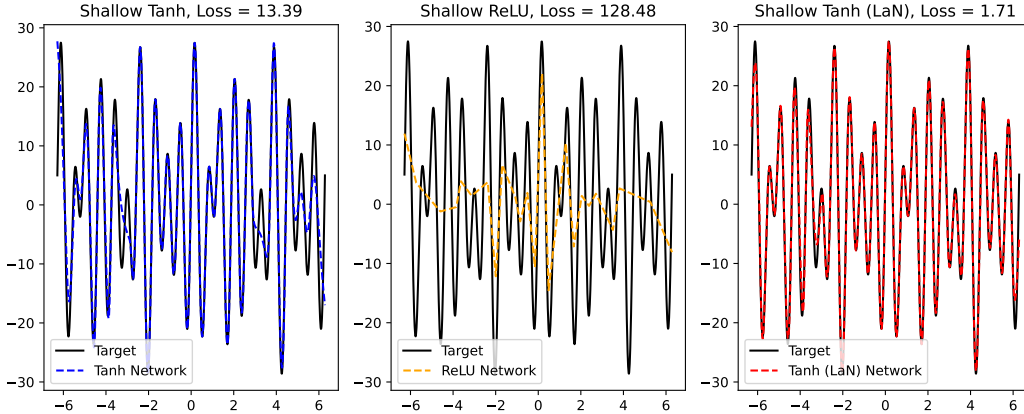


Figure 2: A regression of three shallow neural network architectures on a complex sinusoidal function ($y = 10 * \text{torch.sin}(7 * x) + 15 * \text{torch.sin}(10 * x) + 5 * \text{torch.cos}(5 * x)$). The Tanh (LaN) network emerges as the strongest function approximator, even while having less trainable parameters (501 vs 601 for Tanh & ReLU). To make a fair comparison, the Tanh and ReLU networks have one single hidden layer of size 200, while the Tanh (LaN) network has one single hidden layer of size 100. For the Tanh (LaN) network however, we use two parallel linear layers preceding the hidden layer in order to be able to use the single hidden layer as the product of two activations (see Section 3). For experiments comparing deeper networks, we refer the reader to Appendix C.1.

potentially a strong choice, as it leads to a high effective rank and thus network expressivity (Kumar et al., 2021; Gulcehre et al., 2022).

From the perspective of a compressed representation, defined as the activations of the final hidden layer, we therefore investigate the use and improvement of continuously differentiable activations in the reinforcement learning context. This is done by providing an alternative to the conventional way of parameterizing a representation. Specifically, the following contributions are made to the field:

- We show that, similar to dying ReLU’s, dying hyperbolic tangents are also abundant in the representation when training RL.
- A Latent Assistance Network (LaN) is introduced, modifying the representation of a network to be the product of two separate, individual activations.
- We demonstrate that, without tuning any hyperparameters or using any auxiliary losses, the addition of a LaN yields significant performance gains over using a standard continuously differentiable activation in the Atari domain, and reveal how it decreases dying neurons and increases the internal representations’ effective rank.

2 PRELIMINARIES

We consider an agent acting within its environment, where the environment is modeled as a discrete Markov Decision Process (MDP) defined as a tuple $(\mathcal{S}, \mathcal{A}, T, R, \gamma)$. Here, \mathcal{S} is the state space, \mathcal{A} is the action space, $T : \mathcal{S} \times \mathcal{A} \rightarrow \mathcal{S}$ is the environment’s transition function, $R : \mathcal{S} \times \mathcal{A} \rightarrow \mathcal{R}$ is the environment’s reward mapping and γ is the discount factor. A replay buffer B is used to store visited states $s_t \in \mathcal{S}$ that were followed by actions $a_t \in \mathcal{A}$ and resulted in the rewards $r_t \in \mathcal{R}$ and the next states s_{t+1} . One entry in B contains a tuple of past experience (s_t, a_t, r_t, s_{t+1}) . The agent’s goal is to learn a policy $\pi : \mathcal{S} \rightarrow \mathcal{A}$ that maximizes the expectation of the discounted return $V^\pi(s) = \mathbb{E}_\tau[\sum_{t=0}^{\infty} \gamma^t R(s_t, a_t) \mid s_t = s]$, where τ is a trajectory following the policy π .

Furthermore, we examine the setting where a high-dimensional state ($s_t \in \mathbb{R}^v$) is compressed into lower-dimensional activations $z_t \in \mathcal{Z} = \mathbb{R}^w$ where we call \mathcal{Z} the representation space with $w \leq v$. This is done by means of a neural network encoding $e : \mathcal{S} \rightarrow \mathcal{Z}$ where e represents the encoder.

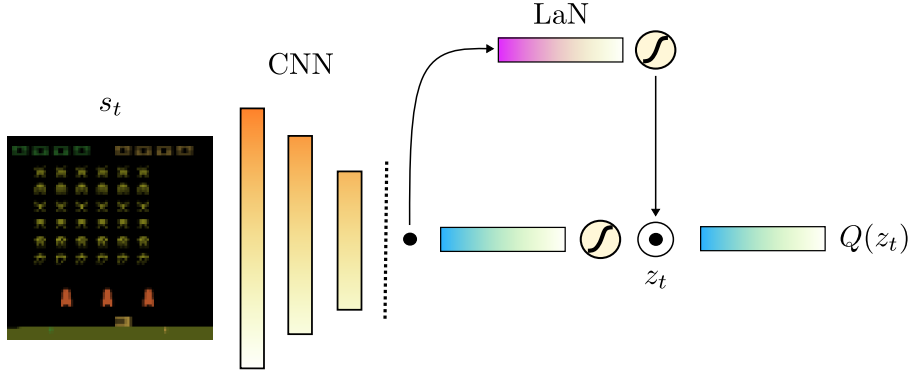


Figure 3: A visualisation of the Latent assistance Network (LaN) architecture combined with the nature DQN architecture applied on a snapshot of the ‘SpaceInvaders’ Atari environment (Mnih et al., 2015). A parallel linear layer providing independent hidden layer activations is integrated, where the element-wise product of the two activations represents the final latent representation z_t used for downstream learning.

3 METHOD

Our method aims at using the symmetrical, stable gradient landscape and the naturally bounded properties of a continuously differentiable activation, while avoiding the pitfalls such as the well-known vanishing gradient problem. To accomplish this, we complement the original linear layer with an additional, independent linear layer. Subsequently, we define the final representation as a product of the two linear layers’ activations. In this section, the continuously differentiable activations as well as the full architecture used in our research are explained.

3.1 CONTINUOUSLY DIFFERENTIABLE ACTIVATIONS

Continuously differentiable activations such as the hyperbolic tangent (\tanh) and the sigmoid (σ) activations are fundamentally different than the $ReLU$ or its Linear-Unit descendants, which are non-symmetric and have a large part of the input space mapped to zero (leading to sparsity). The hyperbolic tangent and the sigmoid output values in the ranges $[-1, 1]$ and $[0, 1]$, respectively. These functions are defined as:

$$\tanh(x) = \frac{e^x - e^{-x}}{e^x + e^{-x}}, \quad \sigma(x) = \frac{1}{1 + e^{-x}} \quad (1)$$

Both functions have the advantage of being differentiable everywhere, as well as being bounded. Furthermore, the sigmoid is well suited for output probabilities, while the tanh is convenient when requiring a zero-centered symmetrical output. However, both functions exhibit the vanishing gradient problem for saturating activations (Glorot & Bengio, 2010; Goodfellow et al., 2016).

3.2 LATENT ASSISTANCE NETWORK (LAN)

To mitigate saturating activations, an augmentation of the conventional representation architecture is proposed. The networks’ original hidden layer is defined as $z^{enc}(x) = f(A_1x + B_1)$, with A_1 and B_1 representing the layer parameters, and with the function $f()$ that represents a nonlinear activation function while x is the set of activations from the previous layer. In order to reduce the number of neurons that are fully saturated (same value for all inputs, similar to collapse), the Latent assistance Network augments the original representation by a parallel representation layer z^* that can be seen as a single highway layer with a closed carry gate (Srivastava et al., 2015). The final representation is defined as the element-wise product between the aforementioned activations:

$$z(x) = z^{enc}(x) \cdot z^*(x) \quad (2)$$

where $z^*(x) = f(A_2x + B_2)$ has A_2 and B_2 that represent the weight matrix and bias. A visualization of the proposed architecture can be found in Fig. 3.

VANISHING GRADIENTS

Our key hypothesis is that the Latent assistance Network can prevent neurons to saturate easily, hence mitigating vanishing gradients. To explain this phenomenon, we investigate the derivative of a product of two functions. For the product of two arbitrary functions $g(x) \cdot h(x)$, the derivative is defined as $g'(x)h(x) + g(x)h'(x)$. In the context of using a sigmoid activation function for $f(x)$, the derivative of $z(x)$ becomes:

$$z'(x) = A_1\sigma(A_1x + B_1)(1 - \sigma(A_1x + B_1))\sigma(A_2x + B_2) + A_2\sigma(A_1x + B_1)\sigma(A_2x + B_2)(1 - \sigma(A_2x + B_2))$$

If a neuron from $f(A_1x + B_1) = 0 \forall x$, the gradient of the product becomes 0 while if a positive saturation is experienced i.e. $f(A_1x + B_1) = 1 \forall x$, $z'(x)$ can remain nonzero. For a product of two hyperbolic tangent functions, the derivative is defined as:

$$h'(x) = A_1\text{sech}^2(A_1x + B_1)\tanh(A_2x + B_2) + \tanh(A_1x + B_1)A_2\text{sech}^2(A_2x + B_2)$$

where sech^2 is the derivate of a hyperbolic tangent. When using a hyperbolic tangent, the key difference with a sigmoid is that for any saturating value of $g(x)$, it will consistently keep the second part of the equation nonzero and dominated by $h(x)$, due to the hyperbolic tangents' saturation into strictly nonzero values. This means that during saturation of a neuron in $g(x)$, the non-saturated function $h(x)$ can still maintain a non-trivial gradient in the product derivative $h'(x)$, thus providing a mechanism to avoid vanishing gradients.

Taking a more formal approximation of neuron collapse through the lens of probability theory, we define the probability of a single neuron saturating as \mathbf{p} . Furthermore, in the case of a sigmoid or hyperbolic tangent, we assume symmetric saturation probabilities to both ends, defining the probability of a neuron saturating to one end of the spectrum as $0.5\mathbf{p}$. Under these assumptions, we show that interpreting a neuron as the product of two individual neurons will change saturation probabilities depending on the neuron activation function. For an overview, we refer the reader to both Table 1 and the corresponding empirical evidence in Appendix C.2.

Hyperbolic Tangent In the case of the hyperbolic tangent, product saturation only occurs if strictly both neurons are saturated. This results in a probability of $\mathbf{p} \cdot \mathbf{p} = \mathbf{p}^2$. Taking a product of hyperbolic tangent activated neurons thus reduces the probability of neuron saturation from \mathbf{p} to \mathbf{p}^2 .

Sigmoid For the sigmoid function, product saturation occurs in two scenarios: Either one of the neurons is saturated towards zero or both neurons are saturated towards 1. The probability that a single neuron does not saturate towards zero is $(1 - 0.5\mathbf{p})$, and subsequently the probability that neither neuron saturates towards zero is $(1 - 0.5\mathbf{p})^2$. The probability that at least one of the two neurons saturates to zero is therefore $1 - (1 - 0.5\mathbf{p})^2 = \mathbf{p} - 0.25\mathbf{p}^2$. Adding the probability that both neurons saturate towards 1, which is $(0.5\mathbf{p})^2 = 0.25\mathbf{p}^2$, the final probability of the neuron product saturation is $\mathbf{p} - 0.25\mathbf{p}^2 + 0.25\mathbf{p}^2 = \mathbf{p}$. Taking a product of sigmoid activated neurons therefore does not reduce the probability of neuron collapse.

ReLU In the case of a ReLU activation, we also assume the probability of a single neuron dying to be \mathbf{p} . As we look at the product of two neurons, the probability that one of the two neurons does not saturate is therefore $1 - \mathbf{p}$, and the probability that both neurons do not saturate is $(1 - \mathbf{p})^2$. The probability that at least one neuron saturates is thus equal to $1 - (1 - \mathbf{p})^2 = 2\mathbf{p} - \mathbf{p}^2$. As the ReLU saturation results in strict zeroes, this results in the product also being zero. Taking a product of ReLU activated neurons therefore increases the final neuron saturation probability from \mathbf{p} to $2\mathbf{p} - \mathbf{p}^2$.

It might seem logical to address neuron saturation by increasing the representation layer size, e.g. doubling it. However, in the experiments section we show that larger layers are not desirable and fail to achieve the unique benefits of the introduced architecture.

Furthermore, the product function $h(x)g(x)$ can exhibit more complex behavior due to the interactions between the input parameters influenced by both functions. These properties are illustrated with a basic regression task in Fig. 2.

Table 1: Summary of dying neuron probabilities with and without a Latent assistance Network (LaN).

Activation Function	Dying Neuron Probability	Probability with LaN	Difference
Hyperbolic Tangent	\mathbf{p}	\mathbf{p}^2	$-(\mathbf{p} - \mathbf{p}^2)$
Sigmoid	\mathbf{p}	\mathbf{p}	0
ReLU	\mathbf{p}	$2\mathbf{p} - \mathbf{p}^2$	$+(\mathbf{p} - \mathbf{p}^2)$

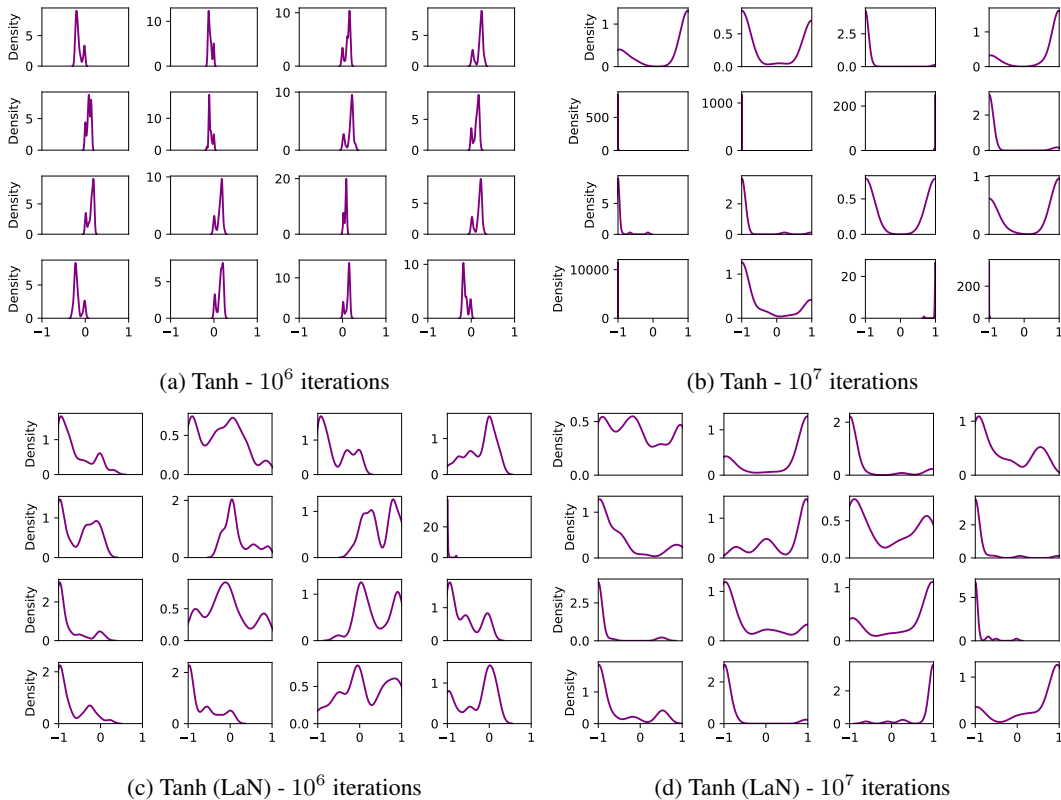


Figure 4: Kernel Density Estimations (KDE) over a subset of 16 neurons in the compressed representation z_t after training DQN in the 'Breakout' environment. Each neuron represents one dimension of the representation $z_t \in \mathbb{R}^{512}$. The representation using a LaN tends to more quickly utilize the full range of the hyperbolic tangent and strongly mitigates dying neurons as compared to using a single hyperbolic tangent. Furthermore, using a LaN leads to more multimodal density distribution as compared to using a regular hyperbolic tangent. More information on the neuron KDE's can be found in Appendix B.

DYING HYPERBOLIC TANGENTS

Although common literature has focused on the dying ReLU problem (He et al., 2015; Lu et al., 2019; Gulcehre et al., 2022; Sokar et al., 2023), we find that representations activated by hyperbolic tangents tend to also show strong dying neuron behavior. Given that the hyperbolic tangent is an asymptotic function near its saturation point, the classification of its saturation remains qualitative. In order to combine visualization and neuron classification, we approximate the amount of dying hyperbolic tangents by applying a Kernel Density Estimation (KDE) to the activations $\alpha_i, i \in \mathbb{R}^w$ of each individual neuron in the compressed representation z_t . More details of the KDE calculation and neuron classification can be found in Appendix B. For the visualization of the representation layer, a fixed subset of the neurons α_i is taken. For both an encoder with and without using a LaN, we provide a visualization of sixteen individual neuron KDE's in Fig. 4.

4 EXPERIMENTS

We conduct our main experiments and discussion on the Deep Q-Learning algorithm (DQN) by Mnih et al. (2015) in Atari, and complement them by additionally evaluating the LaN on the Proximal Policy Optimization algorithm (PPO) (Schulman et al., 2017). In all experiments, we build on the strong baseline implementations from `cleanrl` (Huang et al., 2022). For both DQN and PPO, we define the representation z_t as the last hidden layer of the network, which serves as the compressed representation of the original pixel observation s_t (see Fig. 3). Using a LaN, we show that it is possible to decrease dying hyperbolic tangents while respectively increasing the effective rank of the representation z_t , as well as downstream performance.

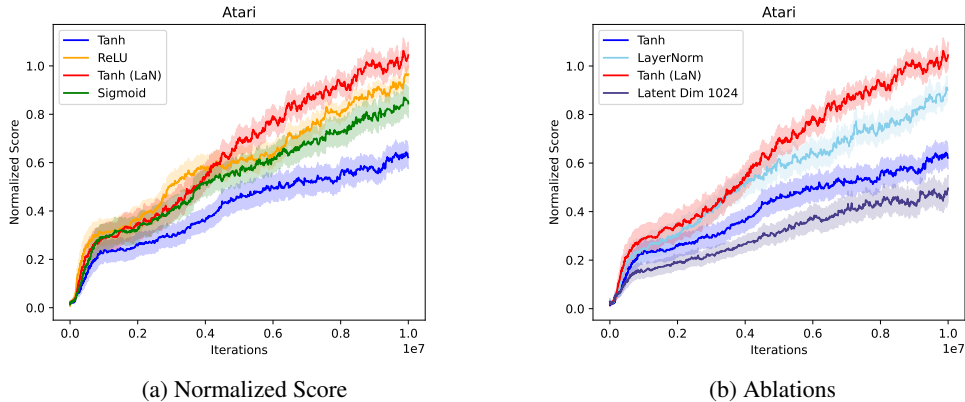


Figure 5: Normalized performance with the standard deviation over the means in the Atari domain, after training DQN for 10M iterations (40M Frames). In (a), a product of hyperbolic tangents is the only continuously differentiable activation that performs equal or better than the ReLU activation, without any hyperparameter changes. Furthermore, using a product of hyperbolic tangent representations seems to greatly outperform the single hyperbolic tangent. In (b), several ablations including layer normalization (Ba et al., 2016) on hyperbolic tangent activations are shown. Notably, the decrease in performance when using a single hyperbolic tangent with a twice as large representation ($z_t \in \mathbb{R}^{1024}$) shows that more parameters are not always desirable.

We perform all experiments on 8 common, non-exploration driven Atari games. We normalize using the ReLU baseline normalized scores and show in Appendix D.1 that human-normalized scores provide an even better score for Tanh (LaN), due to the strong LaN performance in one of the games where humans perform much worse.

REINFORCEMENT LEARNING

In DQN, the action a_t is chosen following an ϵ -greedy policy. With probability ϵ , a random action is selected, and with $(1 - \epsilon)$, the action maximizing the Q-value is chosen. The target Y_t is defined as:

$$Y_t = r_t + \gamma Q'(z_{t+1}, \arg \max_{a \in \mathcal{A}} Q(z_{t+1}, a)), \quad (3)$$

where $Q'(z, a)$ denotes the target Q-network, an auxiliary network that stabilizes the learning by providing a stable target for $Q(z, a)$. The parameters of Q' are updated less frequently to enhance learning stability. The loss function for training the network is:

$$\mathcal{L}_Q = |Y_t - Q(z_t, a)|^2. \quad (4)$$

Proximal Policy Optimization (PPO) operates on a different principle, utilizing policy gradient methods for policy improvement. PPO seeks to update the policy by maximizing an objective function while preventing large deviations from the previous policy through a clipping mechanism in the objective’s estimator. The clipped policy gradient loss L^{CLIP} is defined as:

$$L^{CLIP}(\theta) = \mathbb{E} \left[\min(r_t(\theta)\hat{A}_t, \text{clip}(r_t(\theta), 1 - \epsilon, 1 + \epsilon)\hat{A}_t) \right], \quad (5)$$

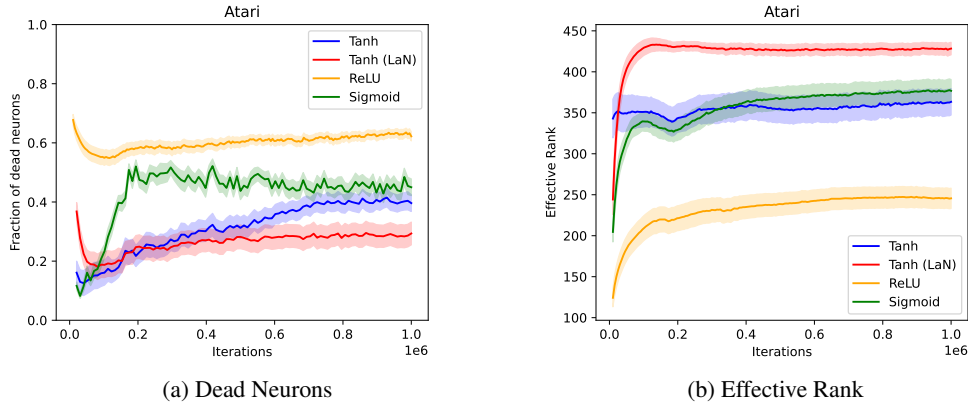


Figure 6: The average fraction of dead neurons (a) and the average effective rank (Kumar et al., 2021) (b) of the representation z_t when training DQN in the Atari domain for 10M iterations (40M frames). Similar to the well-known dying ReLU problem, hyperbolic tangent and sigmoid activations also exhibit strong dying neuron behavior when training RL. Furthermore, a product of hyperbolic tangents reduces dead neurons in z_t and subsequently increases the effective rank of the representation.

where $r_t(\theta)$ represents the ratio of the probabilities under the new policy versus the old policy, and \hat{A}_t is the advantage estimate at timestep t . This clipped surrogate objective ensures gradual and stable policy updates.

4.1 ATARI - DQN

The influence of a LaN on downstream performance can be seen in Fig. 5. A significant improvement over the standard hyperbolic tangent baseline is seen, as well as an important improvement over the strong ReLU baseline. Examining further ablations in Fig. 7 shows that using a sophisticated Linear-Unit function such as the SELU activation (Klambauer et al., 2017) or using an addition rather than a product of hyperbolic tangents seems detrimental to performance. Furthermore, taking a product of 3 hyperbolic tangents ($2 \times \text{LaN}$) also appears to enhance performance, though the improvement is not significantly different from using a single LaN. This could be the result of increased contracting behavior in the early stage of training due to subsequent multiplication of activations whose absolute values are < 1 . Further experiments combining the ReLU activation with a LaN can be found in Appendix C.3.

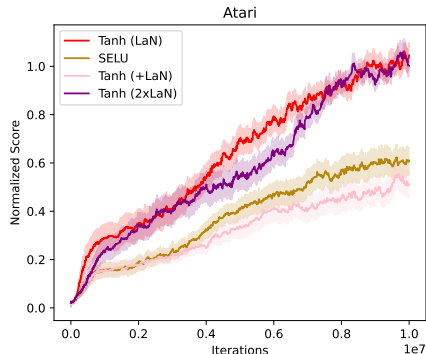


Figure 7: Additional ablations run on DQN in the Atari domain. Tanh (+LaN) represents an addition rather than an elementwise product with a LaN, and Tanh ($2 \times \text{LaN}$) uses two Latent assistance Networks.

MITIGATING DYING HYPERBOLIC TANGENTS

As mentioned in Section 3, the number of dead neurons is defined as the amount of neurons that display the same output for any given observation s_t . The amount of dead neurons over time when training on Atari can be seen in 6a. For the ReLU activation, around 60% of the neurons in the representation z_t are dead, while for the sigmoid and hyperbolic tangent activation this number is around 40%. When using a hyperbolic tangent with a LaN, a reduction in dead neurons as compared to using a single hyperbolic tangent or sigmoid can be observed. We credit this to the inherent ability of a product of hyperbolic tangents to minimize long-term activation saturation, as explained in Section 3. This reduction of long-term dead hyperbolic tangents when using the LaN is remarkable as it is also coinciding with a stronger divergence of values in the initial stages of training (see Fig. 4).

INCREASING EFFECTIVE RANK

We calculate the effective rank (Kumar et al., 2021) of the representation z_t during training, which can be seen in Fig. 6b. As observed by Gulcehre et al. (2022), a representation activated by a hyperbolic tangent or, residing in the same category, a sigmoid, already has a relatively high effective rank compared to a representation activated by a ReLU. Furthermore, as can additionally be seen in supervised learning (see Fig. 2), a LaN notably improves the effective rank of the hyperbolic tangent, which can be seen as a measure of network ‘expressivity’. We summarize our results qualitatively in Table 2.

Table 2: High-level summary of the strengths of a LaN.

Activation function	Performance RL	Few dead neurons	Effective rank
Tanh (LaN)	++	++	++
Tanh	-	-	+
ReLu	+	--	--
Sigmoid	-	-	-

4.2 ATARI - PPO

Additional experiments are run using the PPO algorithm (Schulman et al., 2017). For PPO, the internal architectural difference with DQN is that the compressed representation z_t precedes both a critic and an actor network, and thus receives policy and value gradients (see Appendix A.2). The results can be found in Fig. 8. Similarly to DQN, the Tanh (LaN) exhibits the highest effective rank and the best performance. The Tanh (LaN) and the ReLU also seem to have consistent strong performance across both algorithms, whereas the pure hyperbolic tangent and sigmoid activations are relatively unreliable.

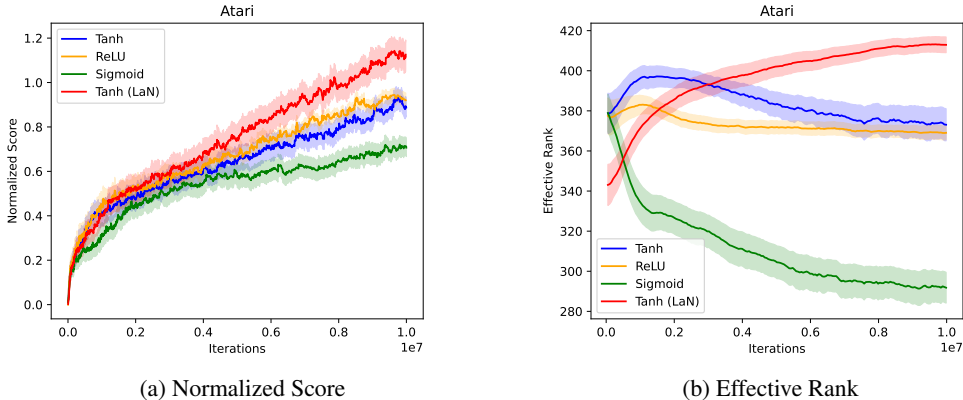


Figure 8: Normalized performance (a) and effective rank (b) in the Atari domain for 10M iterations (40M Frames) when training the PPO algorithm (Schulman et al., 2017).

5 RELATED WORK

Network Capacity in RL. Liu et al. (2019) investigated the need for sparse representations in the continuous control domain. Gulcehre et al. (2022) analyzed network expressiveness in RL by measuring the effective rank (Kumar et al., 2021) of the compressed representation, and found that hyperbolic tangent representations generally maintain high rank and do not suffer strongly from rank decay as training continues. Other work by Lyle et al. (2022) investigated capacity loss in RL and similarly found that, as training progresses, the inherent network capacity of RL algorithms decays. Further research by Nikishin et al. (2022) used network resets to counteract the primacy bias and Sokar et al. (2023) evaluated and mitigated the dying ReLU phenomenon in DQN, both operating in

the sample efficiency setting. Nikishin et al. (2023) further studied plasticity injection for long-term training. In another related direction, recent work has investigated network sparsity in RL, showing that a large part of network capacity might be unnecessary when training reinforcement learning (Graesser et al., 2022; Sokar et al., 2022; Tan et al., 2023; Arnob et al., 2021). This provides further insights into why a ReLU can achieve strong performance despite resulting in a significant number of dead neurons.

Network Architecture The origin of network optimization problems with hyperbolic tangents and sigmoids were empirically investigated by Glorot & Bengio (2010), where, according to the authors, a lot of mystery still surrounds the subject. Work by Srivastava et al. (2015) in supervised learning first looked at the idea of using products of hidden layers together with a ‘gate’ that determined the amount of information flow (Hochreiter & Schmidhuber, 1997). Using these ideas, the Resnet was invented (He et al., 2016). More specific to RL, Henderson et al. (2018) showed differences in RL performances over different network architectures and nonlinear activations. Work by Abbas et al. (2023) successfully applied ReLU concatenation (Shang et al., 2016) to improve continual learning while keeping a similar performance when training from scratch. Finally, recent work by Grooten et al. (2024) investigated raw pixel masking for distractions in RL using a parallel CNN input layer.

6 CONCLUSIONS AND DISCUSSION

We have proposed a novel architecture called the Latent assistance Network (LaN) that augments a networks’ final hidden layer by taking the element-wise product with a parallel, independent hidden layer. We discussed and empirically showed that this decreases the occurrence of dead neurons in the representation z_t , increases network expressiveness, and notably improves performance compared to a single continuously differentiable activation such as the hyperbolic tangent.

Our results also show an important increase in performance over the dominant ReLU activation. This paper therefore remains, to the best of our knowledge, the first to show the possibility of elevating a continuously differentiable activation to and beyond the level of the ReLU. Additionally, it should be recognized that the employed DQN baseline was initially optimized specifically for the ReLU activation function.

As investigated by Kumar et al. (2021), a compressed representation activated by a hyperbolic tangent has a much higher effective rank than the ReLU and could therefore yield stronger network expressiveness. We therefore remain hopeful that the hyperbolic tangent can potentially replace the ReLU in a variety of architectures. Making strong claims in this field however remains challenging, as the success of pruning strategies show that network expressiveness might already be in abundance in some settings (Frankle & Carbin, 2019; Obando-Ceron et al., 2024).

Future work could focus on further identifying the intricacies of this architecture in an attempt to push the potential of continuously differentiable activations in reinforcement learning or even in supervised learning. Also, we believe that an implementation of this architecture in a continual learning setting with similar evaluations as the work in Abbas et al. (2023) could be promising.

7 LIMITATIONS

Our work has focused on the encoders’ final hidden layer in reinforcement learning. As literature suggests that convolutional layers have an even stronger preference for ReLU activations (Jarrett et al., 2009), we have not conducted experiments testing a LaN on the convolutional activations of our encoders.

Due to the heavy computational requirements of the Atari domain, limitations of our work include the use of a moderate amount of 5 seeds per environment, as well as the lack of a hyperparameter search for using the ‘Tanh (LaN)’ setting in our experiment section. A hyperparameter search could further strengthen our results, as the strong baseline is specifically tuned for the ReLU activation. Furthermore, as we perform experiments on DQN and PPO, integration of our Latent assistance Network into more sophisticated algorithms such as Rainbow (Hessel et al., 2018) would be interesting.

REFERENCES

- Zaheer Abbas, Rosie Zhao, Joseph Modayil, Adam White, and Marlos C. Machado. Loss of plasticity in continual deep reinforcement learning. In Sarath Chandar, Razvan Pascanu, Hanie Sedghi, and Doina Precup (eds.), *Proceedings of The 2nd Conference on Lifelong Learning Agents*, volume 232 of *Proceedings of Machine Learning Research*, pp. 620–636. PMLR, 22–25 Aug 2023. URL <https://proceedings.mlr.press/v232/abbas23a.html>.
- Samin Yeasar Arnob, Riyasat Ohib, Sergey M. Plis, and Doina Precup. Single-shot pruning for offline reinforcement learning. *CoRR*, abs/2112.15579, 2021. URL <https://arxiv.org/abs/2112.15579>.
- Jimmy Lei Ba, Jamie Ryan Kiros, and Geoffrey E. Hinton. Layer normalization, 2016. URL <http://arxiv.org/abs/1607.06450>. cite arxiv:1607.06450.
- Shiv Ram Dubey, Satish Kumar Singh, and Bidyut Baran Chaudhuri. Activation functions in deep learning: A comprehensive survey and benchmark. *Neurocomputing*, 503:92–108, 2022. ISSN 0925-2312. doi: <https://doi.org/10.1016/j.neucom.2022.06.111>. URL <https://www.sciencedirect.com/science/article/pii/S0925231222008426>.
- Jonathan Frankle and Michael Carbin. The lottery ticket hypothesis: Finding sparse, trainable neural networks. In *International Conference on Learning Representations*, 2019. URL <https://openreview.net/forum?id=rJl-b3RcF7>.
- Xavier Glorot and Yoshua Bengio. Understanding the difficulty of training deep feedforward neural networks. In Yee Whye Teh and Mike Titterton (eds.), *Proceedings of the Thirteenth International Conference on Artificial Intelligence and Statistics*, volume 9 of *Proceedings of Machine Learning Research*, pp. 249–256, Chia Laguna Resort, Sardinia, Italy, 13–15 May 2010. PMLR. URL <https://proceedings.mlr.press/v9/glorot10a.html>.
- I. Goodfellow, Y. Bengio, and A. Courville. *Deep Learning*. Adaptive computation and machine learning. MIT Press, 2016. ISBN 9780262035613. URL <https://books.google.co.in/books?id=Np9SDQAAQBAJ>.
- Laura Graesser, Utku Evci, Erich Elsen, and Pablo Samuel Castro. The state of sparse training in deep reinforcement learning. In Kamalika Chaudhuri, Stefanie Jegelka, Le Song, Csaba Szepesvari, Gang Niu, and Sivan Sabato (eds.), *Proceedings of the 39th International Conference on Machine Learning*, volume 162 of *Proceedings of Machine Learning Research*, pp. 7766–7792. PMLR, 17–23 Jul 2022. URL <https://proceedings.mlr.press/v162/graesser22a.html>.
- Bram Grooten, Tristan Tomilin, Gautham Vasan, Matthew E. Taylor, A. Rupam Mahmood, Meng Fang, Mykola Pechenizkiy, and Decebal Constantin Mocanu. Madi: Learning to mask distractions for generalization in visual deep reinforcement learning. In *International Conference on Autonomous Agents and Multiagent Systems, AAMAS*, 2024.
- Caglar Gulcehre, Srivatsan Srinivasan, Jakub Sygnowski, Georg Ostrovski, Mehrdad Farajtabar, Matthew Hoffman, Razvan Pascanu, and Arnaud Doucet. An empirical study of implicit regularization in deep offline RL. *Transactions on Machine Learning Research*, 2022. ISSN 2835-8856. URL <https://openreview.net/forum?id=HFfJWx60IT>.
- Kaiming He, Xiangyu Zhang, Shaoqing Ren, and Jian Sun. Delving deep into rectifiers: Surpassing human-level performance on imagenet classification. In *Proceedings of the IEEE international conference on computer vision*, pp. 1026–1034, 2015.
- Kaiming He, Xiangyu Zhang, Shaoqing Ren, and Jian Sun. Deep Residual Learning for Image Recognition. In *Proceedings of 2016 IEEE Conference on Computer Vision and Pattern Recognition*, CVPR ’16, pp. 770–778. IEEE, June 2016. doi: 10.1109/CVPR.2016.90. URL <http://ieeexplore.ieee.org/document/7780459>.
- Peter Henderson, Riashat Islam, Philip Bachman, Joelle Pineau, Doina Precup, and David Meger. Deep reinforcement learning that matters. In *Proceedings of the Thirty-Second AAAI Conference on Artificial Intelligence and Thirtieth Innovative Applications of Artificial Intelligence Conference and Eighth AAAI Symposium on Educational Advances in Artificial Intelligence*, AAAI’18/IAAI’18/EAAI’18. AAAI Press, 2018. ISBN 978-1-57735-800-8.

-
- Matteo Hessel, Joseph Modayil, Hado van Hasselt, Tom Schaul, Georg Ostrovski, Will Dabney, Dan Horgan, Bilal Piot, Mohammad Gheshlaghi Azar, and David Silver. Rainbow: Combining improvements in deep reinforcement learning. In Sheila A. McIlraith and Kilian Q. Weinberger (eds.), *AAAI*, pp. 3215–3222. AAAI Press, 2018. URL <http://dblp.uni-trier.de/db/conf/aaai/aaai2018.html#HesselMHSODHPAS18>.
- Sepp Hochreiter and Jürgen Schmidhuber. Long short-term memory. *Neural Computation*, 9(8): 1735–1780, 1997. doi: 10.1162/neco.1997.9.8.1735.
- Shengyi Huang, Rousslan Fernand Julien Dossa, Chang Ye, Jeff Braga, Dipam Chakraborty, Kinal Mehta, and João G.M. Araújo. Cleanrl: High-quality single-file implementations of deep reinforcement learning algorithms. *Journal of Machine Learning Research*, 23(274):1–18, 2022. URL <http://jmlr.org/papers/v23/21-1342.html>.
- Kevin Jarrett, Koray Kavukcuoglu, Marc’Aurelio Ranzato, and Yann LeCun. What is the best multi-stage architecture for object recognition? In *2009 IEEE 12th International Conference on Computer Vision*, pp. 2146–2153, 2009. doi: 10.1109/ICCV.2009.5459469.
- Günter Klambauer, Thomas Unterthiner, Andreas Mayr, and Sepp Hochreiter. Self-normalizing neural networks. In Isabelle Guyon, Ulrike von Luxburg, Samy Bengio, Hanna M. Wallach, Rob Fergus, S. V. N. Vishwanathan, and Roman Garnett (eds.), *Advances in Neural Information Processing Systems 30: Annual Conference on Neural Information Processing Systems 2017, December 4-9, 2017, Long Beach, CA, USA*, pp. 971–980, 2017. URL <https://proceedings.neurips.cc/paper/2017/hash/5d44ee6f2c3f71b73125876103c8f6c4-Abstract.html>.
- Aviral Kumar, Rishabh Agarwal, Dibya Ghosh, and Sergey Levine. Implicit under-parameterization inhibits data-efficient deep reinforcement learning. In *International Conference on Learning Representations*, 2021.
- Vincent Liu, Raksha Kumaraswamy, Lei Le, and Martha White. The utility of sparse representations for control in reinforcement learning. In *Proceedings of the Thirty-Third AAAI Conference on Artificial Intelligence and Thirty-First Innovative Applications of Artificial Intelligence Conference and Ninth AAAI Symposium on Educational Advances in Artificial Intelligence*, AAAI’19/IAAI’19/EAAI’19. AAAI Press, 2019. ISBN 978-1-57735-809-1. doi: 10.1609/aaai.v33i01.33014384. URL <https://doi.org/10.1609/aaai.v33i01.33014384>.
- Lu Lu, Yeonjong Shin, Yanhui Su, and George E. Karniadakis. Dying relu and initialization: Theory and numerical examples. *CoRR*, abs/1903.06733, 2019. URL <http://dblp.uni-trier.de/db/journals/corr/corr1903.html#abs-1903-06733>.
- Clare Lyle, Mark Rowland, and Will Dabney. Understanding and preventing capacity loss in reinforcement learning. In *International Conference on Learning Representations*, 2022. URL <https://openreview.net/forum?id=ZkC8wKoLbQ7>.
- Volodymyr Mnih, Koray Kavukcuoglu, David Silver, et al. Human-level control through deep reinforcement learning. *Nature*, 518(7540):529–533, 2 2015. doi: 10.1038/nature14236.
- Vinod Nair and Geoffrey E Hinton. Rectified linear units improve restricted boltzmann machines. In *ICML 2010*, pp. 807–814, 2010.
- Evgenii Nikishin, Max Schwarzer, Pierluca D’Oro, Pierre-Luc Bacon, and Aaron Courville. The primacy bias in deep reinforcement learning. In Kamalika Chaudhuri, Stefanie Jegelka, Le Song, Csaba Szepesvari, Gang Niu, and Sivan Sabato (eds.), *Proceedings of the 39th International Conference on Machine Learning*, volume 162 of *Proceedings of Machine Learning Research*, pp. 16828–16847. PMLR, 17–23 Jul 2022. URL <https://proceedings.mlr.press/v162/nikishin22a.html>.
- Evgenii Nikishin, Junhyuk Oh, Georg Ostrovski, Clare Lyle, Razvan Pascanu, Will Dabney, and Andre Barreto. Deep reinforcement learning with plasticity injection. In A. Oh, T. Naumann, A. Globerson, K. Saenko, M. Hardt, and S. Levine (eds.), *Advances in Neural Information Processing Systems*, volume 36, pp. 37142–37159. Curran Associates, Inc., 2023. URL https://proceedings.neurips.cc/paper_files/paper/2023/file/75101364dc3aa7772d27528ea504472b-Paper-Conference.pdf.

-
- Johan Obando-Ceron, Aaron Courville, and Pablo Samuel Castro. In deep reinforcement learning, a pruned network is a good network. *arXiv preprint arXiv:2402.12479*, 2024.
- John Schulman, Filip Wolski, Prafulla Dhariwal, Alec Radford, and Oleg Klimov. Proximal policy optimization algorithms. *ArXiv*, abs/1707.06347, 2017. URL <https://api.semanticscholar.org/CorpusID:28695052>.
- Wenling Shang, Kihyuk Sohn, Diogo Almeida, and Honglak Lee. Understanding and improving convolutional neural networks via concatenated rectified linear units. In Maria Florina Balcan and Kilian Q. Weinberger (eds.), *Proceedings of The 33rd International Conference on Machine Learning*, volume 48 of *Proceedings of Machine Learning Research*, pp. 2217–2225, New York, New York, USA, 20–22 Jun 2016. PMLR. URL <https://proceedings.mlr.press/v48/shang16.html>.
- Ghada Sokar, Elena Mocanu, Decebal Constantin Mocanu, Mykola Pechenizkiy, and Peter Stone. Dynamic sparse training for deep reinforcement learning. In Lud De Raedt (ed.), *Proceedings of the Thirty-First International Joint Conference on Artificial Intelligence, IJCAI-22*, pp. 3437–3443. International Joint Conferences on Artificial Intelligence Organization, 7 2022. doi: 10.24963/ijcai.2022/477. URL <https://doi.org/10.24963/ijcai.2022/477>. Main Track.
- Ghada Sokar, Rishabh Agarwal, Pablo Samuel Castro, and Utku Evci. The dormant neuron phenomenon in deep reinforcement learning. In *Proceedings of the 40th International Conference on Machine Learning, ICML’23*. JMLR.org, 2023.
- Rupesh K Srivastava, Klaus Greff, and Jürgen Schmidhuber. Training very deep networks. In C. Cortes, N. Lawrence, D. Lee, M. Sugiyama, and R. Garnett (eds.), *Advances in Neural Information Processing Systems*, volume 28. Curran Associates, Inc., 2015. URL https://proceedings.neurips.cc/paper_files/paper/2015/file/215a71a12769b056c3c32e7299f1c5ed-Paper.pdf.
- Richard S. Sutton and Andrew G. Barto. *Reinforcement Learning: An Introduction*. The MIT Press, second edition, 2018. URL <http://incompleteideas.net/book/the-book-2nd.html>.
- Yiqin Tan, Pihe Hu, Ling Pan, Jiatai Huang, and Longbo Huang. Rlx2: Training a sparse deep reinforcement learning model from scratch. *CoRR*, abs/2205.15043, 2023. URL <https://arxiv.org/abs/2205.15043>.
- Bing Xu, Naiyan Wang, Tianqi Chen, and Mu Li. Empirical evaluation of rectified activations in convolutional network. *CoRR*, abs/1505.00853, 2015. URL <http://arxiv.org/abs/1505.00853>.

A IMPLEMENTATION DETAILS

A.1 HYPERPARAMETERS

To evaluate, 8 different Atari environments are tested, using 5 different random seeds. For the mean scores, we take the mean over the eight environments. Our normalized score is calculated according to our baseline, the original implementation using a ReLU activation.

All the hyperparameters used in our experiments for DQN and PPO, respectively, are as reported in `cleanrl` (Huang et al., 2022). The hyperparameters can be found in Table 1 and Table 2.

Table 3: DQN Hyperparameters

Hyperparameter	Value	Description
Learning Rate	1×10^{-4}	Learning rate for the optimizer
Discount Factor (γ)	0.99	Discount for future rewards
Replay Memory Size	1,000,000	Size of the experience replay buffer
Mini-batch Size	32	Number of samples per batch update
Target Network Update Frequency	1000	Update frequency for the target network
Initial Exploration	1.0	Initial exploration rate in ϵ -greedy
Final Exploration	0.1	Final exploration rate in ϵ -greedy
Final Exploration Frame	1,000,000	Frame number to reach final exploration
Exploration Decay Frame	1,000,000	Frames over which exploration rate decays
Action Repeat (Frame Skip)	4	Number of frames skipped per action
Reward Clipping	[-1, 1]	Range to which rewards are clipped
Input Dimension	84 x 84	Dimensions of the input image
Latent Dimension	512	Dimension of the latent representation
Input Frames	4	Number of frames used as input
Training Start Frame	80,000	Frame number to start training
Loss Function	Mean Squared Error	Loss function used for updates
Optimizer	Adam	Optimization algorithm used
Optimizer ϵ	10^{-5}	Adam Epsilon

Table 4: PPO Hyperparameters

Hyperparameter	Value	Description
Learning Rate	2.5×10^{-4}	Learning rate for the optimizer
Discount Factor (γ)	0.99	Discount factor for future rewards
Number of Steps	128	Number of steps per environment before update
Anneal LR	True	Whether to anneal the learning rate
GAE Lambda	0.95	Lambda parameter for GAE
Number of Minibatches	4	Number of minibatches to split the data
Update Epochs	4	Number of epochs per update
Normalize Advantage	True	Whether to normalize advantage estimates
Clipping Coefficient	0.1	Clipping parameter for PPO
Clip Value Loss	True	Whether to clip value loss
Entropy Coefficient	0.01	Coefficient for entropy bonus
Value Function Coefficient	0.5	Coefficient for value function loss
Maximum Gradient Norm	0.5	Maximum norm for gradient clipping
Target KL	None	Target KL divergence between updates
Latent Dimension	512	Dimension of the latent representation
Optimizer	Adam	Optimization algorithm used
Optimizer ϵ	10^{-5}	Adam Epsilon

A.2 PPO ARCHITECTURE

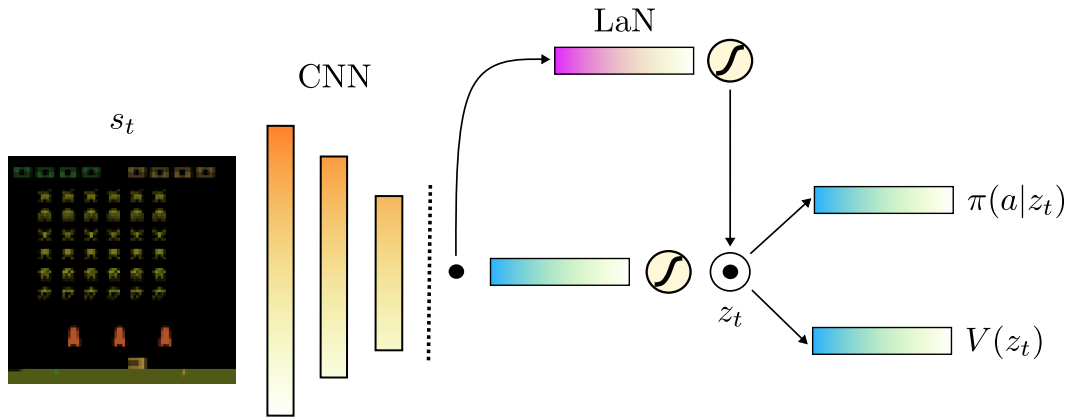


Figure 9: A visualisation of the Latent assistance Network (LaN) architecture combined with the PPO architecture applied on a snapshot of the 'SpaceInvaders' Atari environment. A parallel linear layer providing an independent representation is integrated, where the element-wise product of the two parallel representations represents the final representation z_t .

B KERNEL DENSITY ESTIMATIONS

As discussed in Section 3, we hypothesize that the differences between a hyperbolic tangent with and without a LaN are due to the increased ability of the product of hyperbolic tangents being able to negate dying neurons. We further see this phenomenon when plotting a random selection of neurons from both the mask and the base representation in Fig. 10a.

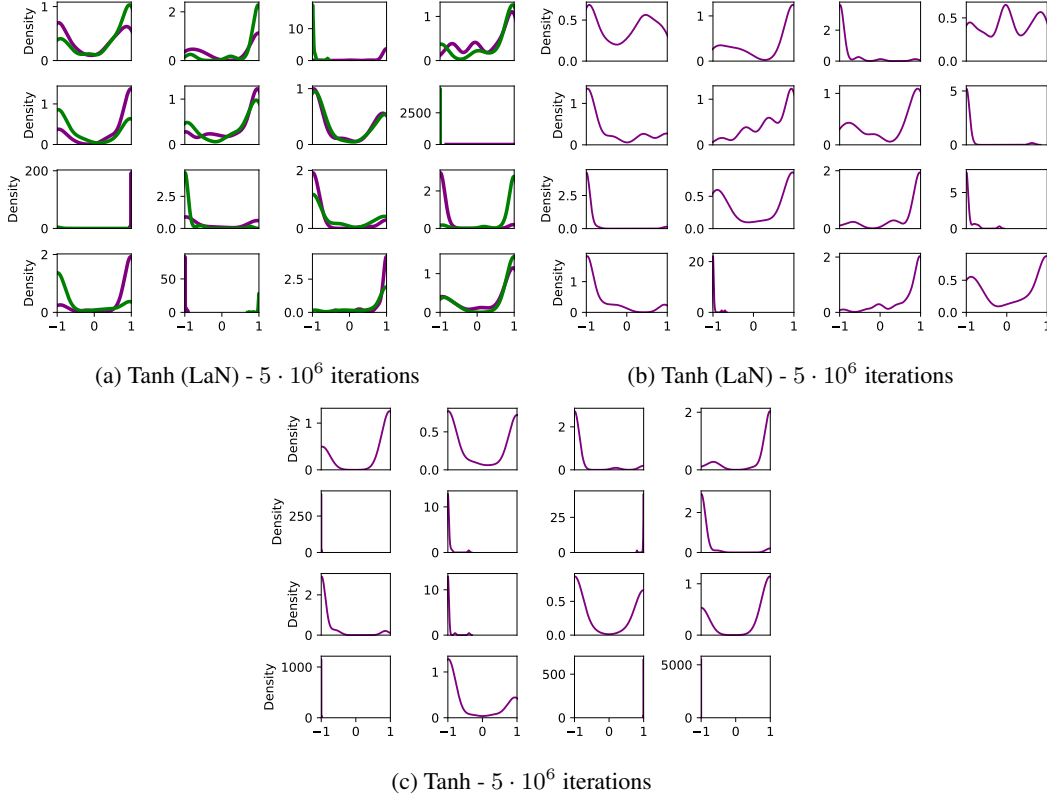


Figure 10: Kernel Density Estimations (KDE) over a subset of 16 neurons in the representations z_t^{enc} and z_t^* in (a), the resulting element-wise product z_t in (b) and the representation z_t when training without a LaN (c). These representations are obtained after training DQN in the 'Breakout' environment. A closer look at neurons 3, 8 and 9 show that when one of the representations saturates, the other is able to compensate, leading to a non-dead neuron in their product z_t .

B.1 KDE CALCULATION

Firstly, to stabilize the KDE computation and avoid singularity issues, a small noise ϵ , following a normal distribution, is added to each neuron's activations:

$$\alpha'_i = \alpha_i + \epsilon, \quad \epsilon \sim \mathcal{N}(0, \sigma^2)$$

where $\sigma^2 = 1 \times 10^{-5}$. The bandwidth for KDE, crucial for the accuracy of the density estimate, is calculated using Scott's rule, adjusted by the standard deviation of the jittered activations:

$$bw = n^{-\frac{1}{5}} \cdot \text{std}(\alpha'_i)$$

where n is the number of samples in α_i . The density of activations is then estimated using a Gaussian kernel:

$$f(x) = \frac{1}{n \cdot bw} \sum_{j=1}^n K\left(\frac{x - \alpha'_{ij}}{bw}\right)$$

Here, K denotes the Gaussian kernel function. In order to finally determine if a neuron is dead, the maximum value of the estimated density function $f(x)$ is compared against a predefined threshold:

$$\max(f(x)) \geq \omega$$

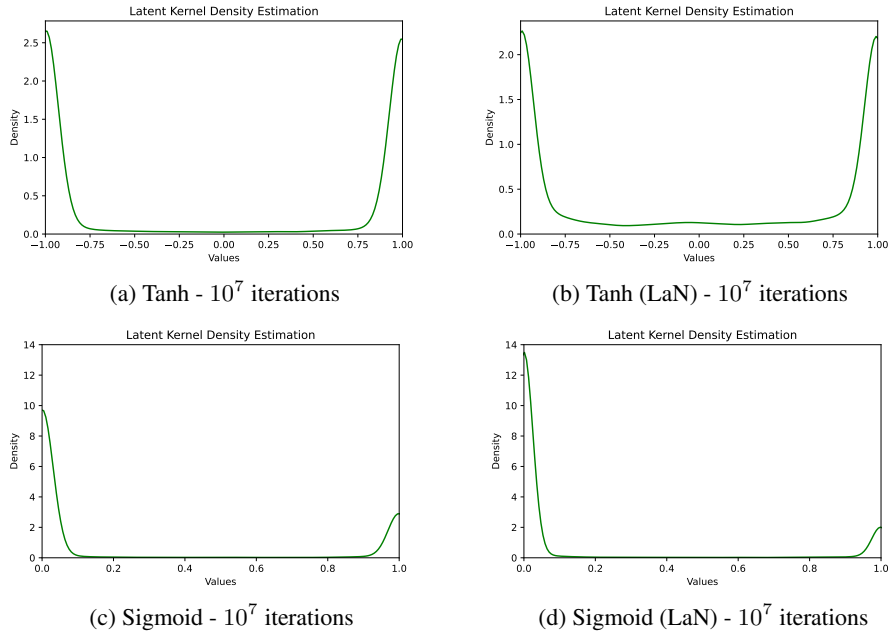


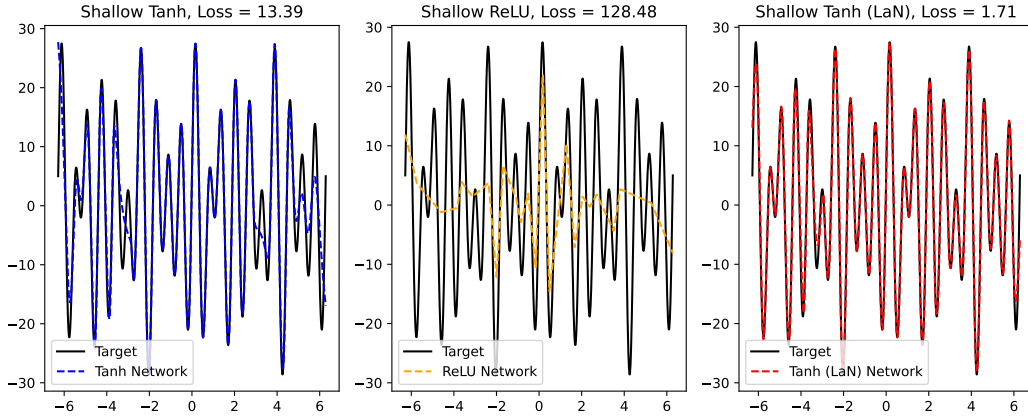
Figure 11: Kernel Density Estimations of the final representation z_t after training DQN for 10^7 iterations in the Breakout environment. A hyperbolic tangent using LaN allows the representation to avoid strong saturation, keeping sufficient kernel density in the central sections of the hyperbolic tangent. As a sigmoid can saturate into zero, using a LaN remains less effective into preventing saturation.

where ω represents the predetermined threshold. In practice, after analyzing the individual neuron KDE's, using an ω of 20 provides a strong approximation of actual dead neurons.

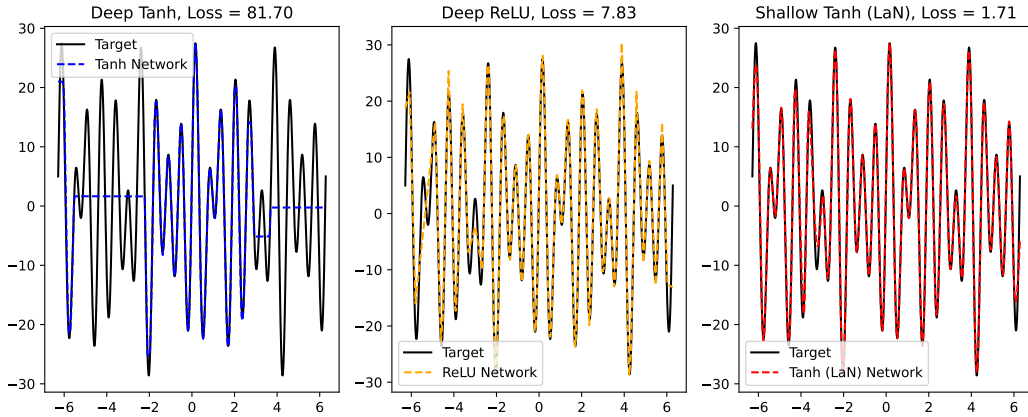
C ADDITIONAL EXPERIMENTS

C.1 SHALLOW AND DEEP FUNCTION APPROXIMATION

To further showcase the effect of activations on complex function approximation, we compare the single hidden layer Tanh (LaN) network from Fig. 2 with a deep ReLU and Tanh network containing three hidden layers each. The comparison with shallow networks can be found in Fig. 12a and a comparison with deep networks can be found in Fig. 12b.



(a) Comparison of shallow networks for a nonlinear regression task. The Tanh and ReLU networks have a single hidden layer of 200 neurons, while the Tanh (LaN) has a single hidden layer of 100 neurons but two preceding linear layers. The Tanh and ReLU networks have 601 parameters, while the Tanh (LaN) network has 501 parameters. As found by Gulcehre et al. (2022), a shallow network activated by ReLU has a lower effective rank and consequently reduced network expressivity as compared to a Tanh activated network. Using a LaN, we achieve better function approximation while using less parameters.



(b) Comparison of two deep networks and one shallow network for the same nonlinear regression task. The Tanh and ReLU networks have 3 hidden layers of 200 neurons each, while the Tanh (LaN) network remains shallow. In line with common observations in deep learning, the ReLU activation thrives in deeper networks, in contrast to the Tanh activation. Interestingly, the shallow Tanh (LaN) network still achieves better function approximation with only 0.6% of the deeper networks' parameters (81001 vs 501). No hyperparameter tuning or architecture search has been applied. Additional tests using deep Tanh (LaN) networks gave similar function approximation as compared to the shallow Tanh (LaN) network.

C.2 VALIDATION OF DYING NEURON PROBABILITY DERIVATIONS

As discussed in Section 3, the effect of adding a Latent assistance Network (LaN) to the original representation strongly depends on the activation function. These derivations are empirically validated by the results in Fig. 13. In practice, since a neural network prefers symmetry, a sigmoid saturates slightly faster to 0 than to 1. This could explain the very slight increase in dead neurons when using a LaN with a sigmoid.

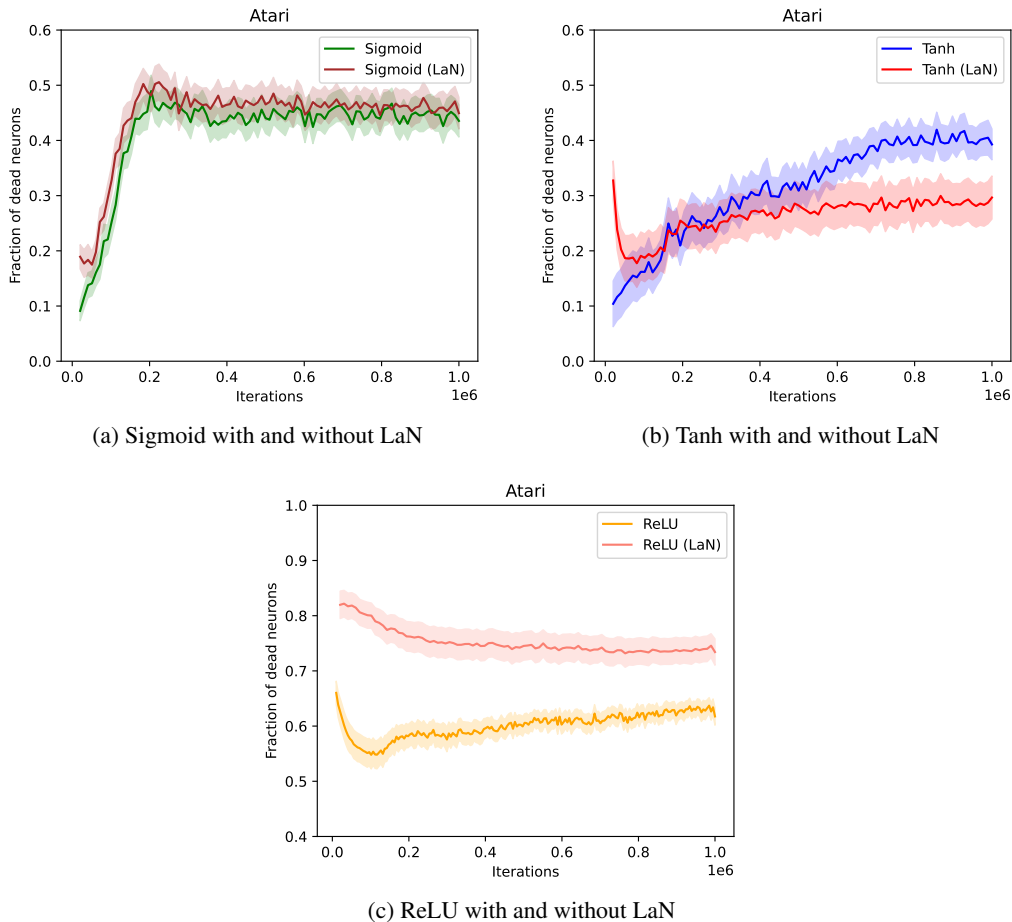


Figure 13: By evaluating the effect of a LaN on dying neurons through the lens of probability theory, we predicted that only the hyperbolic tangent benefits in this metric. Specifically, only a hyperbolic tangent was speculated to have a decrease in dying neurons. Using a LaN on a sigmoid activation would have no notable difference, and for the ReLU activation we expected an increase in dead neurons. This empirically validates our theory in Section 3.

C.3 COMBINING ReLU WITH A LaN

Additional Atari experiments are provided comparing a ReLU activation with and without a LaN. The results can be seen in fig. 14.

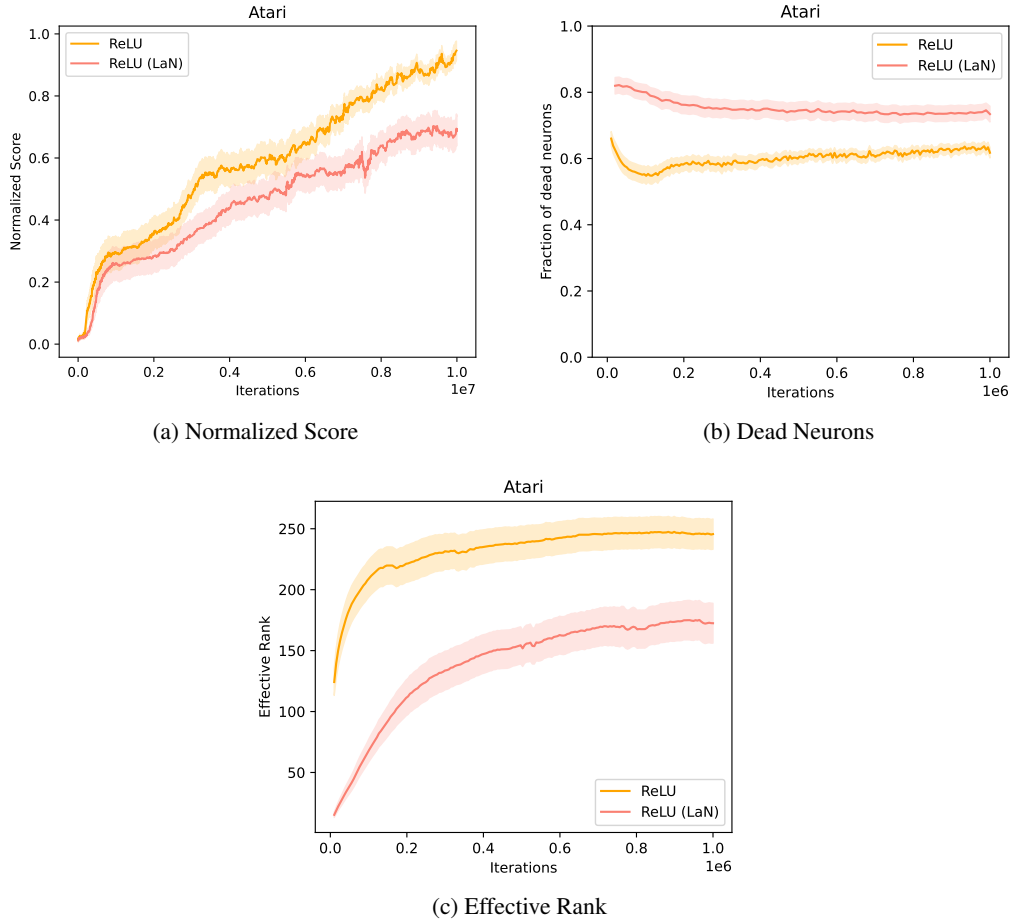


Figure 14: As a Rectified Linear Unit creates sparse representations, it does not benefit from using a LaN, since the final representation will consist of the element-wise product between two sparse representations. Therefore, a decrease in both performance and effective rank and an increase in dead neurons can be expected.

D ATARI

D.1 EVALUATION DETAILS

We normalize performance with respect to the ReLU baseline in `cleanrl` Huang et al. (2022). The minimum and maximum score of the ReLU baseline are taken for each environment, and the normalized score for each environment is calculated as follows:

$$\text{Normalized Score} = \frac{\text{Score} - \text{Min Score}}{\text{Max Score} - \text{Min Score}} \quad (6)$$

where *Score* refers to the raw performance score of the model being evaluated, *Min Score* is a single value representing the lowest score obtained by the ReLU baseline (usually equivalent to random policy or even slightly worse), and *Max Score* is a single value representing the highest score achieved by the ReLU baseline in the same environment. To average, we sum the normalized scores for every run and take the mean.

The more official Human-Normalized Score, as referenced in Mnih et al. (2015), is calculated similarly but using human and random performance benchmarks:

$$\text{Human-Normalized Score} = \frac{\text{Score} - \text{Random Score}}{\text{Human Score} - \text{Random Score}} \quad (7)$$

where *Human Score* and *Random Score* refer to the scores recorded by human players and random agents, respectively. Calculating our performance according to the Human-Normalized Score leads to the plot seen in Fig. 15. Due to taking a subset of the full atari domain, the VideoPinball environment is extremely dominant in the Human-Normalized Score calculation. For a more realistic comparison of the methods, we therefore decided to use baseline-normalized scores in the main paper.

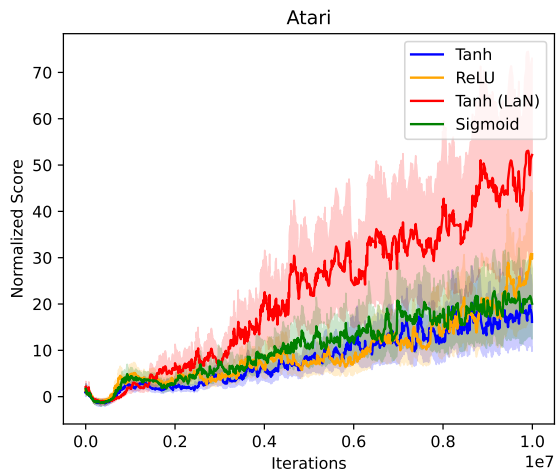


Figure 15: Human-Normalized performance (in multiples) with the standard deviation over the means in the Atari domain for 10M iterations (40M Frames)

D.2 INDIVIDUAL ENVIRONMENTS

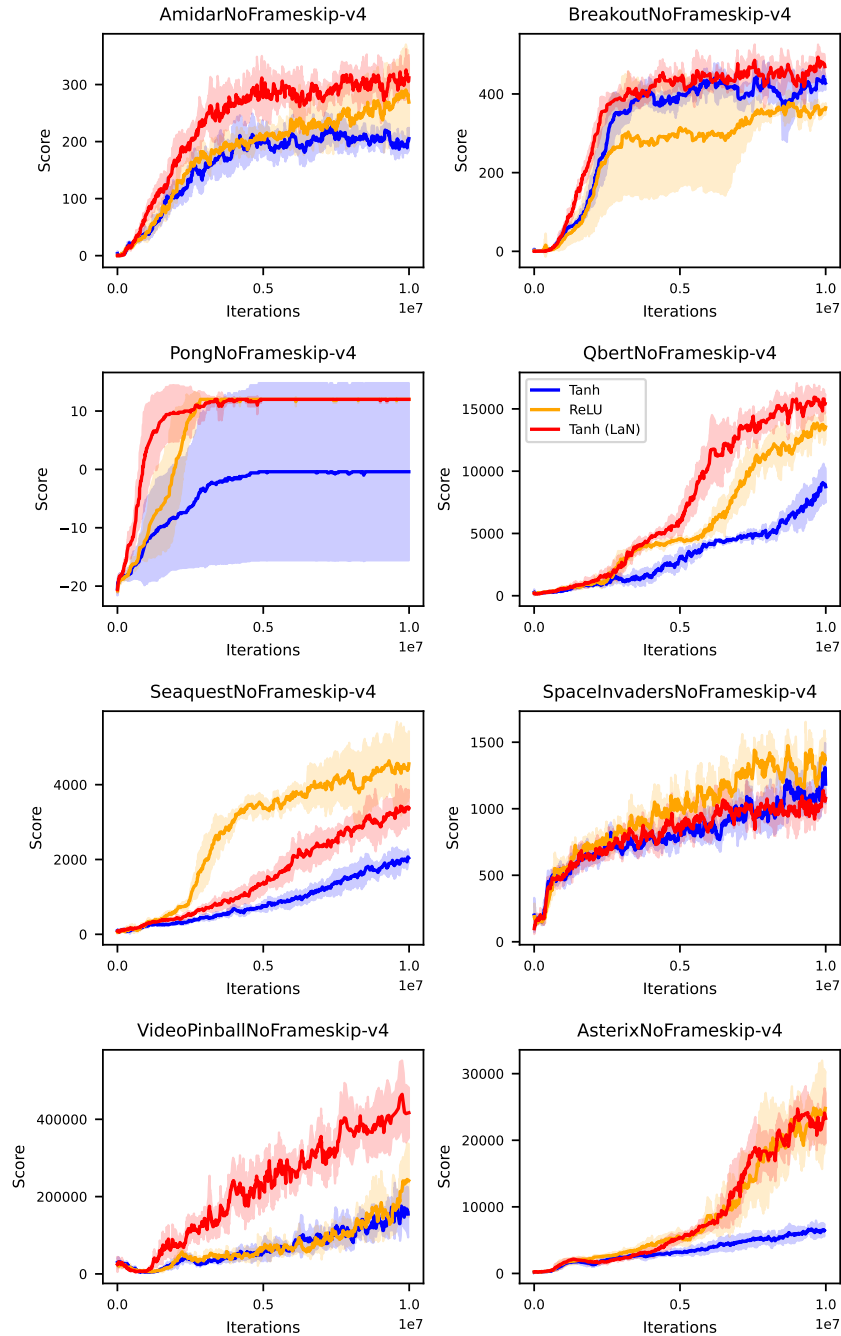


Figure 16: **DQN** Performance comparison on the individual Atari Environments. Plotted lines represent the mean taken over 5 seeds, with the standard deviations expressed as the shaded region. Eight popular Atari games in the RL community that are non-exploration driven were chosen due to computational limitations. To avoid cherry-picking, no other Atari games were tested.

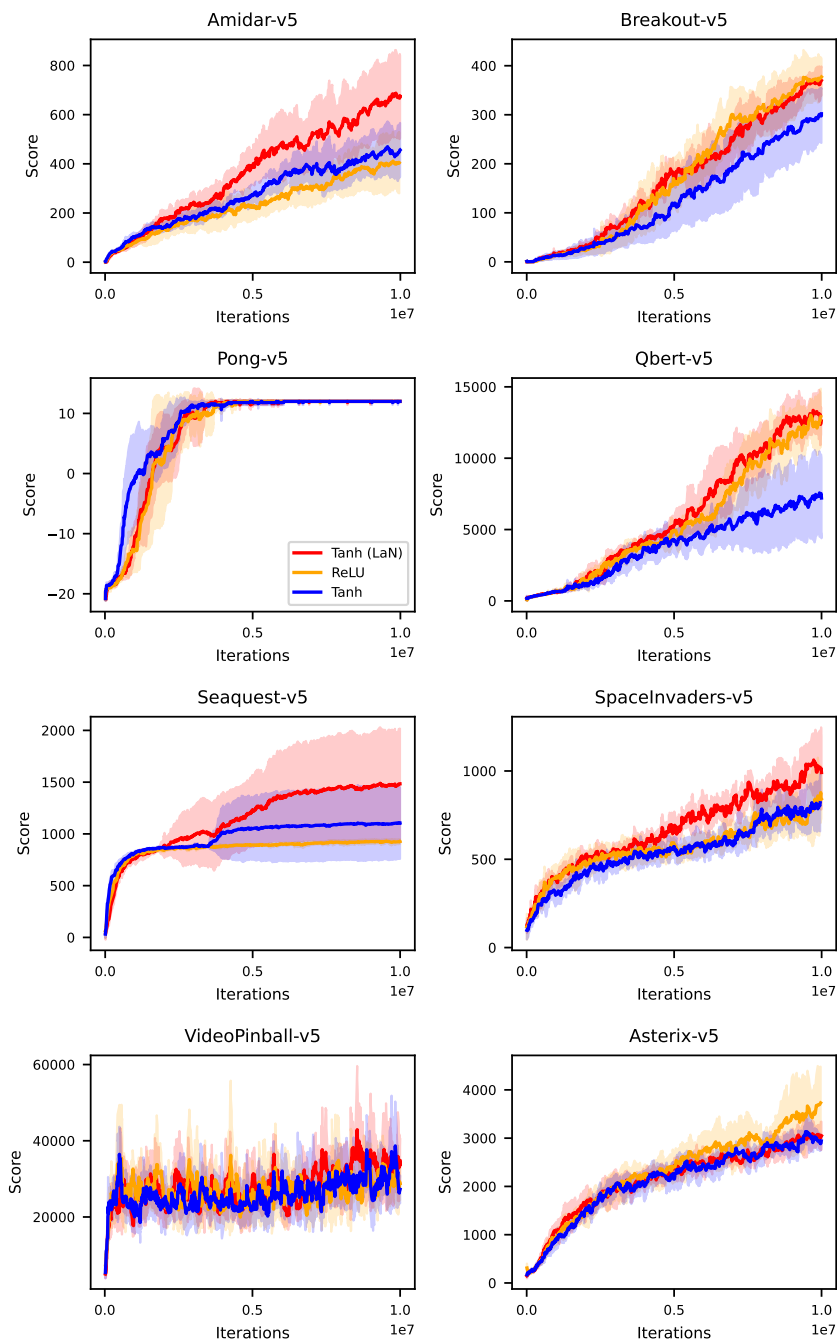


Figure 17: **PPO** Performance comparison on the individual Atari Environments. Plotted lines represent the mean taken over 5 seeds, with the standard deviations expressed as the shaded region. Eight popular Atari games in the RL community that are non-exploration driven were chosen due to computational limitations. To avoid cherry-picking, no other Atari games were tested.